Optical lens-microneedle array for percutaneous light delivery

MOONSEOK KIM,[1,2,7] **JEESOO AN,**[1,7] **KI SU KIM,**[1,7] **MYUNGHWAN CHOI,**[1,3] **MATJAŽ HUMAR,**[1,4,5] **SHELDON J. J. KWOK,**[1,6] **TIANHONG DAI,**[1] AND **SEOK HYUN YUN**[1,6,*]

[1]*Harvard Medical School and Wellman Center for Photomedicine, Massachusetts General Hospital, Cambridge, MA 02139, USA*
[2]*Department of Physics, Korea University, Seoul 136-701, South Korea*
[3]*Department of Biomedical Engineering, Sungkyunkwan University; Center for Neuroscience and Imaging Research, Institute for Basic Science, Suwon, South Korea*
[4]*Condensed Matter Department, J. Stefan Institute, Jamova 39, SI-1000 Ljubljana, Slovenia*
[5]*Faculty of Mathematics and Physics, University of Ljubljana, Jadranska 19, SI-1000, Ljubljana, Slovenia*
[6]*Harvard-MIT Health Sciences and Technology, Cambridge, MA 02139, USA*
[7]*These authors contributed equally*
[*]*syun@mgh.harvard.edu*

Abstract: The limited penetration depth of light in skin tissues is a practical bottleneck in dermatologic applications of light-induced therapies, including anti-microbial blue light therapy and photodynamic skin cancer therapy. Here, we demonstrate a novel device, termed optical microneedle array (OMNA), for percutaneous light delivery. A prototype device with a 11 by 11 array of needles at a spacing of 1 mm and a length of 1.6 mm was fabricated by press-molding poly-(lactic acid) (PLA) polymers. The device also incorporates a matched microlens array that focuses the light through the needle tips at specific points to achieve an optimal intensity profile in the tissue. In experiments done with bovine tissues, the OMNA enabled us to deliver a total of 7.5% of the input photons at a wavelength of 491 nm, compared to only 0.85% without the device. This 9-fold enhancement of light delivery was close to the prediction of 10.8 dB by ray-tracing simulation and is expected to increase the effective treatment depth of anti-microbial blue light therapy significantly from 1.3 to 2.5 mm in human skin.

References and links

1. V. Ntziachristos, "Going deeper than microscopy: the optical imaging frontier in biology," Nat. Methods **7**(8), 603–614 (2010).
2. P. Agostinis, K. Berg, K. A. Cengel, T. H. Foster, A. W. Girotti, S. O. Gollnick, S. M. Hahn, M. R. Hamblin, A. Juzeniene, D. Kessel, M. Korbelik, J. Moan, P. Mroz, D. Nowis, J. Piette, B. C. Wilson, and J. Golab, "Photodynamic therapy of cancer: an update," CA Cancer J. Clin. **61**(4), 250–281 (2011).
3. Z. Huang, H. Xu, A. D. Meyers, A. I. Musani, L. Wang, R. Tagg, A. B. Barqawi, and Y. K. Chen, "Photodynamic therapy for treatment of solid tumors--potential and technical challenges," Technol. Cancer Res. Treat. **7**(4), 309–320 (2008).
4. H. Chung, T. Dai, S. K. Sharma, Y.-Y. Huang, J. D. Carroll, and M. R. Hamblin, "The nuts and bolts of low-level laser (light) therapy," Ann. Biomed. Eng. **40**(2), 516–533 (2012).
5. Y. Zhang, Y. Zhu, A. Gupta, Y. Huang, C. K. Murray, M. S. Vrahas, M. E. Sherwood, D. G. Baer, M. R. Hamblin, and T. Dai, "Antimicrobial blue light therapy for multidrug-resistant Acinetobacter baumannii infection in a mouse burn model: implications for prophylaxis and treatment of combat-related wound infections," J. Infect. Dis. **209**(12), 1963–1971 (2014).
6. ICNIRP, "Guidelines on limits of exposure to laser radiation of wavelengths between 180 nm and 1,000 μm," Health Phys. **105**, 271–295 (2013).

7. F. Zhang, V. Gradinaru, A. R. Adamantidis, R. Durand, R. D. Airan, L. de Lecea, and K. Deisseroth, "Optogenetic interrogation of neural circuits: technology for probing mammalian brain structures," Nat. Protoc. **5**(3), 439–456 (2010).
8. R. M. Verdaasdonk and C. F. van Swol, "Laser light delivery systems for medical applications," Phys. Med. Biol. **42**(5), 869–894 (1997).
9. M. A. Kosoglu, R. L. Hood, Y. Chen, Y. Xu, M. N. Rylander, and C. G. Rylander, "Fiber optic microneedles for transdermal light delivery: ex vivo porcine skin penetration experiments," J. Biomech. Eng. **132**(9), 091014 (2010).
10. W. Small 4th, P. R. Buckley, T. S. Wilson, J. M. Loge, K. D. Maitland, and D. J. Maitland, "Fabrication and characterization of cylindrical light diffusers comprised of shape memory polymer," J. Biomed. Opt. **13**(2), 024018 (2008).
11. C. Kim, H. Park, and H. Lee, "Comparison of laser-induced damage with forward-firing and diffusing optical fiber during laser-assisted lipoplasty," Lasers Surg. Med. **45**(7), 437–449 (2013).
12. M. A. Kosoglu, R. L. Hood, J. H. Rossmeisl, Jr., D. C. Grant, Y. Xu, J. L. Robertson, M. N. Rylander, and C. G. Rylander, "Fiberoptic microneedles: novel optical diffusers for interstitial delivery of therapeutic light," Lasers Surg. Med. **43**(9), 914–920 (2011).
13. M. Choi, J. W. Choi, S. Kim, S. Nizamoglu, S. K. Hahn, and S. H. Yun, "Light-guiding hydrogels for cell-based sensing and optogenetic synthesis in vivo," Nat. Photonics **7**(12), 987–994 (2013).
14. M. Choi, M. Humar, S. Kim, and S.-H. Yun, "Step-index optical fiber made of biocompatible hydrogels," Adv. Mater. **27**(27), 4081–4086 (2015).
15. S. Nizamoglu, M. C. Gather, M. Humar, M. Choi, S. Kim, K. S. Kim, S. K. Hahn, G. Scarcelli, M. Randolph, R. W. Redmond, and S. H. Yun, "Bioabsorbable polymer optical waveguides for deep-tissue photomedicine," Nat. Commun. **7**, 10374 (2016).
16. J. Yu, Y. Zhang, Y. Ye, R. DiSanto, W. Sun, D. Ranson, F. S. Ligler, J. B. Buse, and Z. Gu, "Microneedle-array patches loaded with hypoxia-sensitive vesicles provide fast glucose-responsive insulin delivery," Proc. Natl. Acad. Sci. U.S.A. **112**(27), 8260–8265 (2015).
17. S. P. Sullivan, D. G. Koutsonanos, M. Del Pilar Martin, J. W. Lee, V. Zarnitsyn, S.-O. Choi, N. Murthy, R. W. Compans, I. Skountzou, and M. R. Prausnitz, "Dissolving polymer microneedle patches for influenza vaccination," Nat. Med. **16**(8), 915–920 (2010).
18. P. C. DeMuth, Y. Min, B. Huang, J. A. Kramer, A. D. Miller, D. H. Barouch, P. T. Hammond, and D. J. Irvine, "Polymer multilayer tattooing for enhanced DNA vaccination," Nat. Mater. **12**(4), 367–376 (2013).
19. M. T. C. McCrudden, E. McAlister, A. J. Courtenay, P. González-Vázquez, T. R. Singh, and R. F. Donnelly, "Microneedle applications in improving skin appearance," Exp. Dermatol. **24**(8), 561–566 (2015).
20. J.-H. Park, M. G. Allen, and M. R. Prausnitz, "Biodegradable polymer microneedles: fabrication, mechanics and transdermal drug delivery," J. Control. Release **104**(1), 51–66 (2005).
21. J. H. Park, Y. K. Yoon, S. O. Choi, M. R. Prausnitz, and M. G. Allen, "Tapered conical polymer microneedles fabricated using an integrated lens technique for transdermal drug delivery," IEEE Trans. Biomed. Eng. **54**(5), 903–913 (2007).
22. V. T. Valerii, "Light scattering study of tissues," Phys. Uspekhi **40**(5), 495–515 (1997).
23. A. N. Bashkatov, E. A. Genina, and V. V. Tuchin, "Optical properties of skin, subcutaneous, and muscle tissues: A review," J. Innov. Opt. Health Sci. **04**(01), 9–38 (2011).

1. Introduction

The transport distance of light in biological tissues is limited by scattering and absorption. The optical penetration depth, which is defined as the depth at which light intensity is attenuated to 1/e (~37%), is 0.1-1 mm for visible light in 400-600 nm and 2-3 mm for near-infrared light in 700-1300 nm for human skin [1]. The fluence rate of therapeutic light is limited to prevent undesirable photothermal damage of tissues. Given the maximum permissible exposure (MPE) levels and the optical attenuation in human skin, current phototherapies, such as photodynamic therapy (PDT) [2, 3] and low-level light therapy [4], can only be used to treat lesions in shallow, superficial layers of human skin tissue.

Anti-microbial blue light therapy is currently under preclinical development [5]. This technique uses blue light to treat infections in skin and other tissues affected by drug-resistant pathogenic bacteria. Studies have shown that blue light can kill *Pseudomonas aeruginosa* and *Acinetobacter baumannii* with negligible side effects on surrounding skin tissues. The mechanism of cytotoxic action relies on the light activation of porphyrin or flavin molecules that are endogenously present in the bacteria. These photosensitizer molecules have absorption peaks in the blue wavelengths at 405-470 nm. Typically an optical fluence level of ~50 J/cm^2 at 415 nm is necessary for successful bacteria eradication at depths of 50 µm in the murine epidermis *in vivo* [5]. Considering the MPE level of 200 mW/cm^2 for human skins,

the maximum therapeutic depth for blue light therapy is limited to only ~1 mm, which is insufficient for most practical applications in human patients [6].

Several techniques to overcome this light delivery problem have been reported. Optical fibers and fiber-optic microneedles have been used to deliver visible and near-infrared light to interstitial tissues with improved efficiencies [7–9]. Optical diffusers were attached to the tips of the optical fibers to diffuse light to wide illuminated areas and prevent photothermal tissue damage by otherwise concentrated light at the tips [10–12]. Implantable light-guiding hydrogels have also been developed for on-demand activation of optogenetic cells *in vivo* to synthesize therapeutic proteins [13]. Step-index optical fibers made of hydrogels with functionalized core and clad structures have been developed for *in vivo* applications [14]. Recently, thin planar waveguides made of biodegradable polymers permitted photochemical tissue bonding of deep (1-2 cm) skin incisions [15].

In this study, we describe a novel optical microneedle array (OMNA) for antimicrobial blue light therapy. The design of our prototype is optimized for the dermatologic applications of blue-light therapy and photodynamic therapy in human skin. Our work was inspired by the recent development of microneedle arrays for drug delivery [16], vaccination [17, 18], and cosmetic skin treatments [19], applications that do not require optically transparent microneedles. To the best of our knowledge, optically functioning microneedles have not previously been reported.

2. Design and fabrication

Our OMNA device consists of a microneedle array and a microlens array (Fig. 1(a)). In our prototype, these two parts were prepared separately and bonded together, although they could in principle be fabricated as a single unit. The purpose of the microlens array is to focus incoming light into each microneedle at appropriate converging angles to reduce insertion loss and enable propagation of incoming light along each microneedle (Fig. 1(b)). The light propagating inside each microneedle is extracted into the surrounding tissue (Fig. 1(c)). In this present study, the design of OMNA was optimized for blue light therapy at depths up to 2.5 mm below the tissue surface.
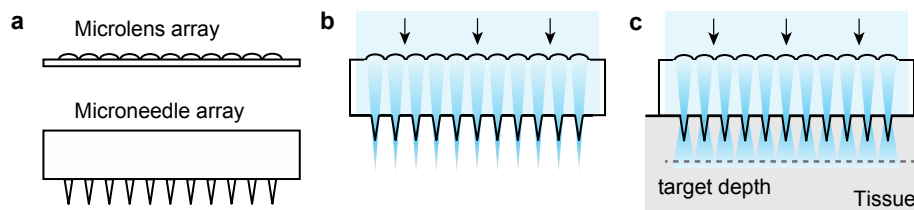

Fig. 1. Design principle of the OMNA. (a) Schematics of a microneedle array and microlens array. (b) Illustration of an assembled OMNA. The microlens array focuses incident light through the microneedles. (c) Illustration of light delivery into a tissue. The design has been optimized to achieve uniform and maximal light intensity at a target depth.

For blue light therapy, the microneedles should be made of a material that is transparent, mechanically strong and, preferably, biocompatible to avoid inducing adverse immune and inflammatory reactions in the skin. To satisfy this requirement, we selected poly(lactic acid) (PLA) with a molecular weight of about 500 kDa. The refractive index of PLA was measured to be 1.47, and the optical absorption coefficient (μ_a) was 0.014 mm^{-1} at an optical wavelength (λ) higher than 400 nm. PLA offers a high Young's modulus of ~3.5 GPa, which is sufficient for insertion into skin tissues.

We used a mold made of poly(dimethyl siloxane), PDMS, with a negative pattern of the microneedles. Pellets of PLA were placed onto the PDMS mold in a vacuum oven at 150 °C for 15 min. The temperature was then increased to 200 °C for 30 min, during which the PLA pellets were melted on the mold. The bubbles in the PLA melt were removed in a low vacuum

condition (50%) for 10 min. A flat PDMS substrate was placed on top of the melted PLA for 10 min. The mold and substrate were flipped over and incubated in a high vacuum condition for 1 h and were placed in a fridge (2 °C) for 30 min. The solidified PLA microneedle array was then extracted from the mold.

Figure 2(a) shows the fabricated PLA microneedle array. The dimensions of the substrate is 15 mm by 15 mm, with a thickness of 4 mm. The substrate supports 11 by 11 microneedles over an area of 1 cm^2 with a uniform needle spacing of 1.0 mm. Each needle has a length of 1.6 mm and a linear tapered shape with a diameter of 500 µm at the base and ~20 µm at the tip (Fig. 2(b)). The axial force exerted to each needle during insertion is estimated to be 0.05 N [20]. According to an elastic buckling model [21], the base diameter of the conical needle should be larger than 340 µm to avoid buckling. The base size of 500 µm used in our prototype provides sufficient rigidity. The specific dimensions of the microneedle array have been optimized to numerical simulations described in Section 4.
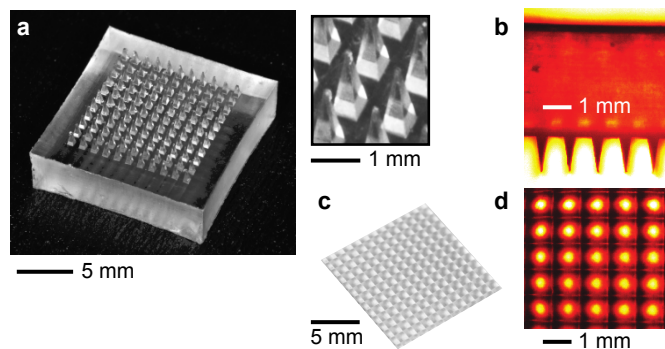

Fig. 2. (a) Photographs of a fabricated prototype PLA microneedle array. (b) An optical side-view transmission image of the microneedle array. Needle length: 1.6 mm, base diameter: 500 µm, interspacing: 1 mm, number of needles: 11 by 11, and substrate size: 15 mm by 15 mm × 4 mm. (c) Photograph of a microlens array. Focal length of lens: 9.5 mm, and substrate size: 15 mm by 15 mm by 2 mm. (d) Optical transmission image of the microlens array.

For microlens array, we made a PDMS mold using a commercially-available microlens array made of fused silica (Flexible Optical B.V.) (Fig. 2(c)), and fabricated PLA microlens arrays with the same protocol used for the fabrication of PLA microneedle arrays. Since only the needles are in contact with tissues, the microlens material needs not be biocompatible. However, PLA is suited for polymer molding and provides perfect index-matching to the PLA microneedle array. The lens spacing of 1 mm was matched to the inter-needle spacing (Fig. 2(d)). The thickness of the microlens array was 2 mm. The focal length of the microlenses was 9.5 mm so that the focal points would be located 1.9 mm beyond the needle tips at a wavelength of 491 nm. Once the optic axis of each lens array was aligned to the microneedle axis (see Section 3 for the alignment procedure in detail), UV-curable transparent optical epoxy (Norland 81) was applied between the microlens array and the microneedle array to bond the two parts together under an UV curing lamp (365 nm, Spectroline, 5 mW/cm^2) for 5 min. The thin epoxy layer with a thickness of < 100 µm and refractive index of 1.56 should cause negligible optical aberration and Fresnel reflection loss (< 0.2%).

3. Optical characterization of the OMNA

An imaging setup was used for the assembly of OMNA and evaluation of the optical transmission loss. The microneedles were pushed against an aluminum foil mask to a controlled distance such that the top 400 µm of the needles penetrated through the foil whereas the rest of the needles remain covered by the foil (Fig. 3(a)). While monitoring the transmission of a collimated laser beam (20 mW, 491 nm, Cobolt) (Fig. 3(b) and

Visualization 1), we used an XYZ translation stage to align the microlenses to the microneedles. After maximum transmission throughout the entire array was achieved, the two pieces were glued using optical epoxy.

The intensity profile of transmitted light through the foil was measured by using a CCD camera with a long depth of focus. Figure 3(c) compares the transmission images of the microneedle array through the foil before and after attaching a microlens array for collimated, coherent laser light at a wavelength of 491 nm. Considerable increase of transmission was apparent. The output intensity at the needle tips was actually higher than the input intensity due to light focusing by the lens array. The varying directions of the optical rays indicate strongly scattered light at the microneedle tip. To collect the scattered light as well in the measurement of total transmittance, we used an integrating sphere (IS200-4, Thorlabs). The throughput of the lens-assisted OMNA was 43% or 3.7 dB in terms of insertion loss including 4% reflection from the polymer surface. The transmission is 4 times higher than the transmittance of 11% without the microlens array.

This measurement was repeated for broadband extended light from an LED source with a spectral range of 400-650 nm (MCWHL5-C1, Thorlabs). Relatively uniform, high transmission was achieved throughout the entire microneedles. The transmission enhancement by the microlens array compared to without the lens array was 3-folds (Fig. 3(d)). The slightly small difference compared to 4% for collimated laser is probably due to the finite range of incidence angle of the LED light. The theoretical angular tolerance of the OMNA was ~4.8°. This can be improved by decreasing the total thickness of the device.
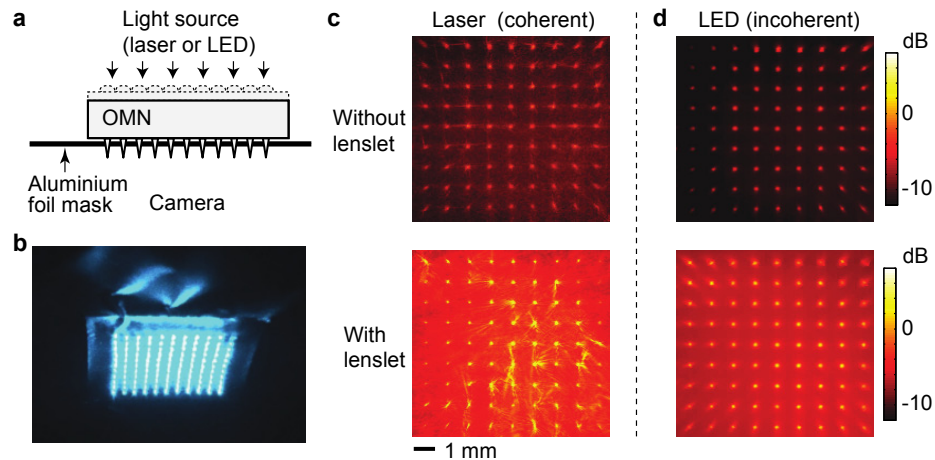

Fig. 3. Light transmission through an assembled OMNA. (a) A setup to align the microlens array and microneedles. Aluminium foil is used to block the beams transmitted outside the needles. (b) A transmission pattern of blue laser light (491 nm) through an optimally aligned OMNA. (Visualization 1: Optimization of alignment) (c-d) Optical images of collimated 491-nm laser light transmitted through a microneedle array without a microlens array (c) and through a lens-assisted OMNA (d). (e-f) Optical transmission images of white LED light through the microneedle array alone (e) and through the lens-assisted OMNA (f). The total amount of transmission was 11%, 43%, 7.7%, and 25% in (c), (d), (e), and (f) respectively. Color bar represents light intensity normalized to the incident light. Color bar represents the optical intensity in a log scale normalized to the input.

4. Numerical simulation

To optimize the optical design, we performed numerical optical simulations using non-sequential ray tracing (Zemax) based on a Monte-Carlo method. To obtain the optical properties of tissue, we prepared sliced bovine and porcine muscle tissues and first characterized their scattering properties by using a setup with a laser beam (λ = 491 nm) and double integrating sphere (IS200-4, Thorlabs) [22, 23]. The tissue samples were sandwiched

between a pair of glass slides with a specific gap distance. The transmittance was measured with a collimated laser beam with a size of 1 mm. Diffusive transmittance T_d, diffusive reflectance R_d were measured with a thin diffuser placed in front of the sample. Using the Kubelka-Munk formalism [22, 23], we obtained the values for scattering coefficient μ_s, anisotropy factor g, absorption coefficient μ_a, and optical penetration depth, $\delta = (3\mu_a(\mu_a + \mu_s(1-g)))^{-0.5}$: for bovine muscles, $\mu_s = 7.9 \pm 0.05$ mm^{-1}, $g = 0.83 \pm 0.01$, $\mu_a = 0.58 \pm 0.05$ mm^{-1}, and $\delta = 550 \pm 50$ μm; and for porcine muscles, $\mu_s = 10.4 \pm 0.05$ mm^{-1}, $g = 0.89 \pm 0.01$, $\mu_a = 0.27 \pm 0.05$ μm^{-1}, $\delta = 960 \pm 130$ μm. The absorption of the bovine tissue was about twice higher than the porcine tissue due to higher blood concentration, which led to shorter light penetration. These values agree well with previously reported values [23].

In the simulation, we used the measured data of bovine muscles, with a refractive index $n = 1.4$ and the Henyey-Greenstein phase function, $p(\theta) = (4\pi)^{-1}(1-g^2)(1 + g^2 - 2g\cos\theta)^{3/2}$ where θ is the scattering angle. We considered collimated laser light (491 nm) with a Gaussian beam profile with a full-width-at-half-maxima size of 10 mm. Direct illumination of the laser beam onto the tissue surface resulted in optical intensity profiles with expected exponential decays over depth (Fig. 4(a)). At the target depth of 2.5 mm, the average optical intensity was 0.73% (−21.4 dB) of the light intensity at the tissue surface (Fig. 4(b)).

Optical simulation with an OMNA in place improved light delivery considerably. In the optimized design described above, the incident beam is focused by the microlens array to a focal point at a depth of 3.5 mm, or 1.9 mm below the needle tip (Fig. 4(c)). Placing the focal plane away from the microneedle tip prevents the beam from forming a tight focus within the tissue and, thereby, helps to avoid photo-damages at the foci. Furthermore, the extended focal length helps to increase the effective depth of light delivery. The intensity distribution at the depth between 1.2 mm and 2.5 mm within the tissue is similar or higher than the order of −10 dB of the incident light. The optical intensity measured at the target depth of 2.5 mm below the tissue surface was 8.7% (−10.6 dB) of the input intensity at the top surface of the OMNA (Fig. 4(d)). In other words, optical simulation predicted a 12-fold (10.8 dB) enhancement of light delivery by the OMNA.
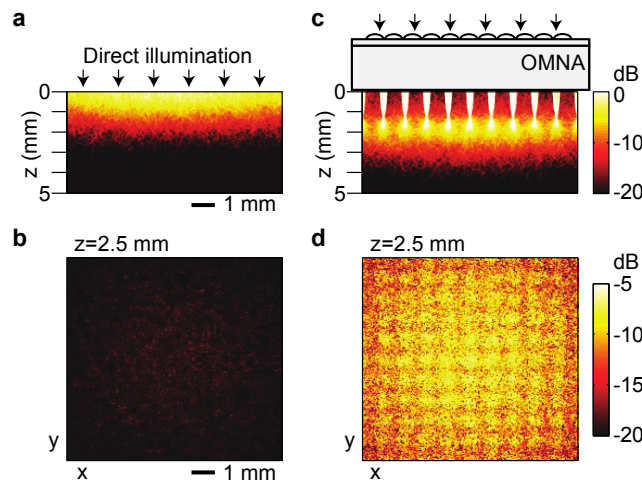

Fig. 4. Numerical simulations of light intensity in tissues. (a, b) Direct illumination of collimated light at 491 nm to the surface of a tissue in a vertical plane (a) and a cross-sectional plane at a depth of 2.5 mm (b). (c, d) Light illumination through an OMNA device in a vertical plane (c) and a cross-sectional plane at the same tissue depth (d). Light delivery efficiency at z = 2.5 mm is 0.73% in (b) and 8.7% in (d). Color bar represents light intensity normalized to the incident light. Intensity in log scale.

5. Measurement of light penetration into tissues

We used a CCD camera to image the transmission profile of a laser beam (λ = 491 nm) through tissues. Figure 5(a) shows the image of a bovine muscle slice with a thickness of 3.1 mm. The total transmission over a central area of 10 mm by 10 mm was only 0.85% when the laser beam was directly illuminated to the tissue (Fig. 5(b)). The transmission increased to 8.5% with the OMNA (Fig. 5(c)), by a factor of 8.9. Figure 5(d) shows a typical transmission image of a 2.7-mm-thick porcine muscle tissue slice. The transmission was 7.6% without (Fig. 5(e)) and 32% with the OMNA (Fig. 5(f)).
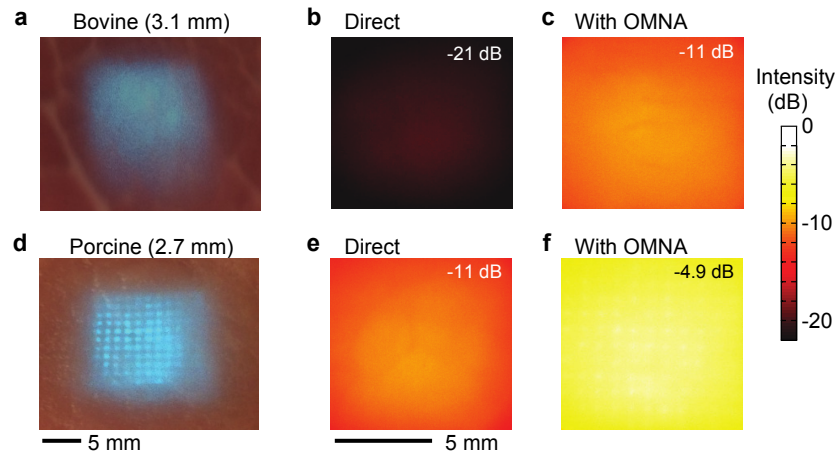

Fig. 5. Enhancement of light penetration into tissues by OMNA. (a-c) Optical penetration through a 3.1-mm-thick bovine tissue slice: (a) Camera image of the tissue; Transmission intensity maps without (b) and with (c) the OMNA. (d-f) Optical transmission through a 2.7-mm-thick porcine tissue slice: (d) Camera image; Transmission intensity maps without (e) and with (f) the OMNA. The magnitudes of transmission are indicated in (c), (d), (e), and (f).

The experimental data agreed remarkably well with our Monte-Carlo ray simulation results (Fig. 6). The optical intensity in the dB scale decreases linearly with the penetration depth, with a slope given by the specific optical properties of the tissue. The OMNA increases the optical intensity at depth effectively by replacing the tissue with transparent needles. From the experimental and simulation data, the effective increase of optical penetration depth was about 1.3 mm, which is slightly shorter than the actual needle length of 1.6 mm. This small discrepancy is attributed to the dispersed beam geometry along the microneedles.
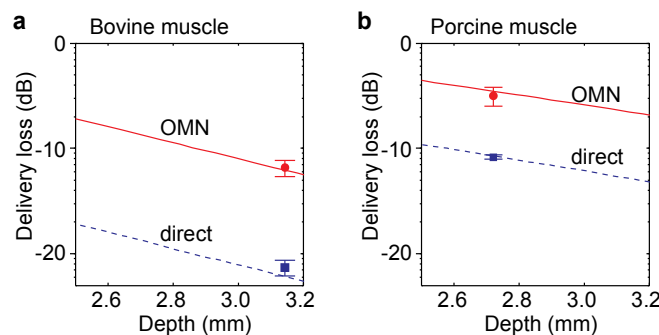

Fig. 6. Ray-optics simulation results of light delivery loss as a function of depths in tissues. (a) Optical intensity in the bovine tissue. (b) Optical intensity in the porcine tissue. Blue dotted lines, simulation data without OMNA. Red lines, simulation data OMNA. Blue rectangles, experimental data in Figs. 5(b) and 5(e). Red circles, experimental data in Figs. 5(c) and 5(f).

6. The effective depth of blue-light therapy

The typical optical dose for blue light therapy required to eradicate *P. aeruginosa* is about 50 J/cm^2 [5]. To provide this therapeutic dose at target depths within the tissue, much higher optical fluence is needed at the skin surface. We calculated the required fluence level at the tissue surface for specific target depths by using ray optics simulation for the human skin tissues, which have typical penetration depths of δ = 220-280 μm at λ = 415 nm [23]. Our results (Fig. 7) showed that the therapeutic depths limited by the maximum power exposure level of the human skin are about 1.2-1.5 mm, whereas the maximum therapeutic depths are extended to 2.4-2.6 mm with the OMNA.
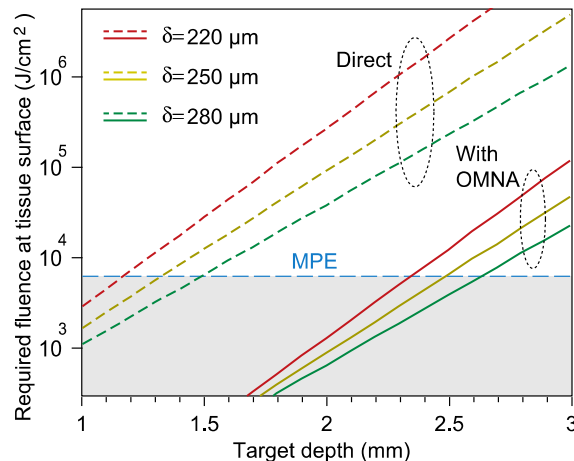

Fig. 7. Required optical fluence at the surface of the human skin to achieve a typical antibacterial therapeutic dose of 50 J/cm^2 at various depths in the tissue. Dashed lines, direct illumination without an OMNA. Solid lines, light delivery with an OMNA. MPE: maximum permissible exposure level at λ=415 nm.

7. Conclusion

We have demonstrated an optimized lens-assisted OMNA for blue-light delivery to a target depth of 2.5 mm in tissues. Compared to direct surface illumination, this novel device enabled to achieve a 9-fold enhancement of light delivery at the target depth. The measured optical intensity profiles in tissues agreed well with numerical ray-optics simulations. Although our present work is optimized to obtain uniform light distribution at maximal intensity at a certain depth, the design parameters of OMNA may be optimized for specific requirements for the optical wavelength, tissue type, and therapeutic depth range. For example, the optical intensity between the tissue surface and the needle tip can be enhanced, if required, by reducing the area and filling ratio of the lens allowing part of light bypass the lens and enter the tissue surface. By extending the effective therapeutic depth, our OMN device can be broadly applied to improve the efficacy of existing phototherapies, such as blue light therapy for antimicrobial treatment and photodynamic therapy for cancerous lesions.